

## Online Methods

### Mice

C57BL/6J, C57BL/6-FoxP3-GFP (B6.Cg-Foxp3<sup>tm1Mal</sup>/J), *Tcr $\alpha$* <sup>-/-</sup> (B6.129S2-Tcratm1Mom/J), *Add2*<sup>-/-</sup> (B6.129S4-*Add2*<sup>tm1Llp</sup>/LlpJ)<sup>51</sup>, *Padi4*<sup>-/-</sup> (B6.Cg-*Padi4*<sup>tm1.1Kmw</sup>/J)<sup>52</sup> mice were purchased from The Jackson Laboratory (Bar Harbor, ME). YAe62 $\beta$  mice have been previously described<sup>53</sup>. For flow cytometric analysis mice both male and female mice were analyzed between 1-8 weeks of age. For deep sequencing experiments, male and female mice were used at 2 and 8 weeks of age. Bone marrow chimeric mice were generated as previously described<sup>53</sup>, and analyzed at 6-8 weeks post transfer. Mice expressing FoxP3-GFP and the YAe62 TCR $\beta$  chain, and all mouse sub-lines were maintained in a specific pathogen-free environment in accordance with institutional guidelines in the Animal Care Facility at the University of Massachusetts Medical School.

### Antibodies

anti-TCR $\beta$  (clone H57-597) cat# 109220; anti-CD62L (clone MEL-14) cat# 104424, anti-PD-1 (clone 29F.1A12) cat# 135210, anti-CD25 (clone PC61) cat# 102038, anti-Nrp1 (clone 3E12) cat# 145211, anti-H-2 K<sup>b</sup> (clone AF6-88.5) cat# 116515, anti-GITR (clone DTA-1) cat# 126318, anti-FR4 (clone 12A5) cat# 125009, anti-CD73 (clone TY/11.8) cat# 127223, anti-XCR1 (clone ZET) cat# 119505, anti-CD5 (clone 53-7.3) cat# 100624 Biologend; anti-CD4 (clone GK1.5) cat# 552051, anti-mV $\alpha$ 2 (clone B20.1) cat# 562944, anti-CD44 (clone IM7) cat# 560780, anti-CTLA4 (clone UC10-4F10-11) cat# 553720, anti-CD11c (clone HL3) cat# 562454, anti-CD11b (clone M1/70) cat# 557657, anti-CD23 (clone B3B4) cat# 553139 BD Pharmingen; anti-CD8 (clone 5H10) cat# MCD0817 ThermoFisher; anti-B220 (clone RA3-6B2), anti-Foxp3 (clone FJK-16s), anti-CD69 (clone H1.2F3), anti-F4/80 (clone BM8) cat# 25-4801-82, anti-MHCII (clone M5/114) cat# 50-112-9473, anti-IgM (clone eB121-15F9) cat# 11-5890-82, anti-CD24 (clone M1/69) cat# 47-0242-82, anti-CD19 (clone 1D3) cat# 48-0193-82 eBioscience.

### Cell surface and intracellular staining and tetramer enrichment

Murine thymocytes, lymph node cells and splenocytes from 1-8 weeks old mice were stained with the following cell antibodies: anti-TCR $\beta$  (H57-597), anti-CD62L (MEL-14), anti-PD-1 (29F.1A12), anti-CD25 (PC61), anti-Nrp1 (3E12), anti-H-2 K<sup>b</sup> (AF6-88.5), anti-GITR (DTA-1), anti-FR4 (12A5), anti-CD73 (TY/11.8) Biologend; anti-CD4 (GK1.5), anti-mV $\alpha$ 2 (B20.1), anti-CD44 (IM7), anti-CTLA4 (UC10-4F10-11) BD Pharmingen; anti-CD8 (5H10) ThermoFisher; anti-B220 (RA3-6B2), anti-Foxp3 (FJK-16s), anti-CD69 (H1.2F3) eBioscience. All antibodies were used at a 1:300 dilution unless otherwise stated. Tetramer staining was carried out in the presence of 50nM dasatinib (Sigma), cells were incubated with dasatinib for 30min at 37c, then incubated for 2hrs with 10 $\mu$ g/mL MHCII tetramer at 37c with additional antibodies added for the last 30min. For intracellular CTLA-4 levels, cells were fixed and permeabilized using the FoxP3 Transcription factor staining buffer set (eBiosciences) at 4c following the manufactures protocol, and subsequently stained overnight with anti-CTLA-4 (1:200 dilution) and anti-Foxp3 (1:200 dilution) at 4c. Analysis of flow cytometric data was performed using FlowJo version 9.9.6 (TreeStar). For analyses of IA<sup>b</sup>-Add2 specific T cells using tetramer enrichment, thymocytes and splenocytes were incubated with 10 $\mu$ g/ml IA<sup>b</sup>-Add2 tetramer coupled to PE for 60min at 22c, then column enriched using anti-PE MACS beads (Miltenyi Biotech) following established protocols<sup>54</sup>. An example of tetramer analyses is shown in Supplementary Fig. 7.

### **Thymocyte, T cell and APC sorting**

Thymocytes and splenocytes were freshly isolated from  $TCRC\alpha^{+/-}$ .Foxp3-GFP and  $TCRC\alpha^{+/-}$ .YAE62b.Foxp3-GFP mice, and sorted for thymic CD4SP and splenic CD4  $T_{conv}$  cells ( $TCR\beta^{+}$ ,  $CD4^{+}$ ,  $CD8^{neg}$ ,  $CD25^{neg}$ , Foxp3-GFP<sup>neg</sup>, B220<sup>neg</sup>) cells, and thymic and splenic  $tT_{reg}$  cells ( $TCR\beta^{+}$ ,  $CD4^{+}$ ,  $CD8^{neg}$ , Foxp3-GFP<sup>+</sup>,  $CD8^{neg}$ , B220<sup>neg</sup>) (FACS Aria, BD Biosciences). In some experiments, thymocytes and splenocytes populations were also sorted using IA<sup>b</sup>-Padi4 tetramer<sup>+</sup> staining. For DC and macrophage subset isolation, spleens were minced, and digested with 2mg/ml Collagenase D (Roche), 20 $\mu$ g/ml DNase 1 (Roche) in RPMI media supplemented with 10% FCS and 0.1 M EDTA for 30min at room temp. Following digestion, splenic slurry was filtered through a 70 $\mu$ m mesh filter, washed and centrifuged over a 15%/12% (w/v) OptiPrep density gradient for 15 min at room temp. and low density cells isolated for flow cytometry sorting. Splenic APC subsets were sorted based on  $CD19^{neg}$   $TCR\beta^{neg}$  and the following cell surface markers; cDC1: MHCII<sup>+</sup>  $CD11c^{+}$   $XCR1^{+}$   $CD11b^{neg}$ ; cDC2: MHCII<sup>+</sup>  $CD11c^{+}$   $XCR1^{neg}$   $CD11b^{low}$ ; Macs:  $CD11b^{hi}$   $F4/80^{+}$   $CD11c^{neg}$ . All B cells were sorted by  $CD19^{+}$   $TCR^{neg}$ , then  $CD5^{hi}$  B cells; remaining  $CD5^{lo}$  B cells were gated for  $CD24^{hi}$  Transitional B cells, while  $CD24^{lo}$  cells were divided into Follicular B cells,  $CD23^{+}$   $IgM^{+}$  and Marginal zone B cells,  $CD23^{lo}$   $IgM^{hi}$ . Thymic APC subsets were enriched by staining with MHCII APC and anti-APC MACS beads (Miltenyi) and subsequently flow sorted using based on  $CD19^{neg}$   $TCR\beta^{neg}$  and the following cell surface markers; pDC:  $CD11c^{lo}$   $B220^{+}$ ; cDC  $CD11c^{+}$   $XCR1^{+}$  and  $CD11c^{+}$   $XCR1^{neg}$ . Thymic B cells were sorted by  $CD19^{+}$   $B220^{+}$   $TCR^{neg}$ . All sorted T cell populations were greater than 99% pure, while APC subsets were greater than 98% pure. All sorted T cell populations were greater than 99% pure, while APC subsets were greater than 98% pure.

### **TCR cloning and generation of T cell transfectomas**

Thymic CD4SP and  $tT_{reg}$  cells were sorted from 2 week old  $TCRC\alpha^{+/-}$ .Foxp3-GFP and  $TCRC\alpha^{+/-}$ .YAE62b.Foxp3-GFP mice. For thymocytes that express the YAE62b chain, cells were directly sorted into Trizol (Invitrogen), RNA was isolated by precipitation with RNase free glycogen (Invitrogen) following the manufacturer's protocol. cDNA was prepared using oligo-dT's (Promega) and Omniscript RT kit (Qiagen). cDNA was PCR amplified for rearranged TCR $\alpha$  chains using a set of PCR primers corresponding to  $V\alpha$  2, 4, 8 and 11 gene families. Amplified rearranged TCR  $V\alpha$  genes were PCR cloned as a fusion with the TCR  $C\alpha$  region into an MSCV based retroviral expression vector. Plasmids were sequenced and only novel TCRs without amplification errors were further studied. For thymocytes that express polyclonal TCR $\beta$  chains, sorted cells were cultured in 24 well plates coated with  $\alpha$ CD3/ $\alpha$ CD28 and 20U/ml of rIL-2 for six days, and converted into hybridomas as previously described<sup>53</sup>. TCR $\beta$  chain gene family use was determined by flow cytometry analyses. To clone TCR $\alpha$  and TCR $\beta$  chains, RNA was isolated from T cell hybridomas, converted to cDNA, and TCR $\alpha$  and TCR $\beta$  chains were PCR amplified using a set of degenerated PCR primers corresponding to all mouse  $V\alpha$  and identified  $V\beta$  gene family. Amplified products were cloned as fusions with the TCR  $C\alpha$  or TCR  $C\beta$  region into an MSCV based retroviral expression vector.

The following PCR primers were used:

$V\alpha 1$  GGG AATTCTCCSTACACATCAGAGACTC

$V\alpha 2$  GGGGGGAGATCTCGAGCCACCATGGACACGATCCTGACAGCA

$V\alpha 4$  GGGGGGAGATCTCGAGCCACCATGGACTCTTCTCCAGGC

V $\alpha$ 8 GGGGGAGATCTCGAGCCACCATGCGTCCTGTACCTGCTCAGTTCTTGTGCTC  
V $\alpha$ 11 GGGGGGAGATCTCGAGCCACCATGCAGAGGAACCTGGGAGCT  
TCR C $\alpha$  CTGGTACACAGCAGGTTCCGGATTCTGGATGT

V $\beta$ 2 GGGGGGAATTCGTCGACGAGCCACCATGTGGCAGTTTTGCATT  
V $\beta$ 4 GGGGGGAATTCGTCGACGAGCCACCATGGGCTCCATTTTCCTC  
V $\beta$ 8 GGGGGGAATTCGTCGACGAGCCACCATGGGCTCCAGACTCTTC  
V $\beta$ 11 GGGGGGAATTCGTCGACGAGCCACCATGGCCCCTAGGCTCCTT  
TCR C $\beta$  - CTTGGGTGGAGTCACATTTCTCAGATCTTC

For T cell transfectoma generation, TCR $\alpha$  or TCR $\beta$  chains were cloned into MSCV based vectors with an IRES element containing resistance genes for puromycin or neomycin, respectively. Retroviral vectors were co-transfected with pCLEco accessory plasmid into the Phoenix packaging line via Lipofectamine 2000 (Life Technologies, Carlsbad, CA). TCR constructs were transduced into CD4<sup>+</sup> T cell hybridoma 5KC-73.8.20 that lacks endogenous TCR $\alpha$  or TCR $\beta$  chains by retroviral spinfection (1000 x g, 2hrs). T cells were selected in 1mg/mL of neomycin or 0.8 $\mu$ g/mL of puromycin for 1 week and stained with anti-TCR $\beta$  antibody (H57-597) to ensure equivalent levels of TCR expression.

### **T cell transfectoma stimulation with APC and peptide library screen**

*In vitro* splenocyte reactivity was determined by incubating 10<sup>5</sup> T cells transfectomas with 5 x 10<sup>5</sup> splenocytes from 6-10 week old naïve C57BL/6 mice or mice that had received 25 $\mu$ g LPS (Sigma) and 100 $\mu$ g anti-CD40 (clone FGK-4.5, Bio-X-cell) i.p. 5 days prior. Supernatants from cultures were screened for IL-2 content using an HT-2 cell based assay bioassay<sup>35</sup>. Analyses of APC subset specific reactivity was determined by culturing 10<sup>5</sup> T cells transfectomas with titrating numbers of cDC1, cDC2, macrophages, and B cell subsets isolated from 6-10 week old naïve C57BL/6 mice or mice that had received LPS and anti-CD40.

To construct an IA<sup>b</sup> self peptide library, we curated mass spectrometry approaches that assessed the IA<sup>b</sup> immunopeptidome of the spleen, LN, thymus, and in LN that drain sites of inflammation in C57BL/6 mice<sup>55-60</sup>. We further accounted for the combined effects of variability in protease cleavage sites and the ability of MHC-II molecules to present peptides with N- and C-terminal extensions. These characteristics of MHC-II peptide presentation allow nested sets of the same self-peptide core sequence to be presented<sup>61</sup>. To limit duplicate self-peptide cores within the library, we synthesized only the largest possible peptide fragment, or when the nested species spanned >18 amino acids, multiple peptide fragments that had an overlap of at least 10 amino acids. This approach reduced the size of the library to ~1750 unique self-peptides (Supplementary Dataset).

To identify peptide ligands recognized by tT<sub>reg</sub> TCRs, 10<sup>5</sup> T cell transfectomas were incubated with 3 x 10<sup>4</sup> of IA<sup>b+</sup> B7.1<sup>+</sup> ICAM-1<sup>+</sup> fibroblasts<sup>35</sup> and 37 $\mu$ g/ml of a mixture of 20 individual peptides (AALabs, San Diego CA) for 24 hrs and analyzed for IL-2 production. Positive responses in the primary screen were confirmed by culturing T cell transfectomas and fibroblasts with titrating amounts of individual soluble peptides. EC<sub>50</sub> values were calculated by fitting to a log (agonist) vs response (three parameters) curve (GraphPad, Prism).

### **TCR clonotype analysis of thymic CD4SP, tT<sub>reg</sub> cells and peripheral tT<sub>reg</sub> cells**

Thymic CD4SP and tT<sub>reg</sub> cells, and splenic CD4<sup>+</sup> T<sub>conv</sub> and CD4<sup>+</sup> tT<sub>reg</sub> cell populations were sorted from 3 replicate groups (3 mice per group) of TCR $\alpha$ <sup>+/-</sup>. YAE62 $\beta$ .Foxp3-GFP

mice to a 98% purity (FACS Aria, BD Biosciences). RNA was isolated using Trizol and precipitated with RNase free glycogen (Invitrogen) following the manufactures protocol. cDNA was prepared using oligo-dT's (Promega) and Omniscript RT kit (Qiagen). cDNA was amplified with 20 rounds PCR with generic

V $\alpha$ 2 primer (5'-CCCTGGGGAAGGCCCTGCTCTCCTGATA-3') and

TCR C $\alpha$  primer (5'-GGTACACAGCAGGTTCTGGGTTCTGGATG-3').

1/10th volume of the first round PCR was amplified with an additional 20 rounds of PCR using barcoded primers, for post sequence identification of originating T cell population, containing Illunima PE read primer and P5/7 regions, respectively. The resulting 300bp fragment was gel purified (Gene Clean II, MP Biomedicals) and sequenced on a MiSeq using a single read 250bp run (Illumina). Sequence data sets were parsed by barcode using the script fastq-multx and clonotypes for each population were tabulated using TCRklass<sup>62</sup>.

For comparing 2wk and 8wk thymic T<sub>reg</sub> frequencies, clonotype counts were summed across replicate datasets. In addition, the counting of each clonotype contained a pseudocount of 1 to act as a buffer when certain clonotypes are not observed in the dataset due to finite sampling of the population (false negatives)<sup>35</sup>. Frequencies for 103 V $\alpha$ 2<sup>+</sup> thymic clonotypes observed in the 2 week old or 8 week old thymic T<sub>reg</sub> datasets were derived from the proportion among the total repertoire of the corresponding age. Padi4-reactive clonal frequencies were determined by averaging V $\alpha$ 2 clonotypes frequencies among 3 replicate deep sequence datasets. For pie charts, the clonal distribution of Padi4-reactive TCRs was determined as a relative proportion of the average frequency for the 5287, 6235, 5290, 4699, 4738, 5292, 6239, 6236, 6256, 6237, 6238 clonotypes.

### **Statistical analysis**

Experimental results were analyzed for significance using one-way ANOVA Tukey multiple comparisons test; unpaired 2-tailed t test; unpaired 2-tailed t test with Welch's correction; non-parametric Dunn's multiple comparison test; one-way ANOVA Sidak's multiple comparison test; Kruskal-Wallis and Dunn's multiple comparisons test. Correlation plots are based on probable cure fit using Akaike's Information Criteria. Specific test to evaluate significance is described in the figure legends. Statistical analyses were performed using Prism v7.04 (Graphpad software). P-values  $\leq 0.05$  were considered significant (\*p $\leq 0.05$ , \*\*p $\leq 0.01$ , \*\*\*p $\leq 0.001$ , \*\*\*\*p $\leq 0.0001$ ) P values  $> 0.05$ ; non-significant (ns)

### **Production of soluble and membrane bound MHC-peptide and TCR proteins**

Soluble and biotinylated pMHC used for SPR, tetramer production and crystallography was produced using the baculovirus expression system and purified as previously described<sup>27, 53</sup>. Soluble TCRs used for surface plasmon resonance experiments and crystallography were expressed in Escherichia coli and refolded as described previously<sup>53</sup>. The TCRs produced in E. coli were murine TCR V $\alpha$  and TCR V $\beta$  domains fused to the human C $\alpha$  and C $\beta$  domains carrying an engineered disulfide bond to improve folding yield and protein stability. TCR $\alpha$  and TCR $\beta$  chains were expressed as inclusion bodies in the BL21 (DE3) strain of E. coli (EMD Millipore, Darmstadt, Germany). Soluble TCRs were produced by refolding mixtures of denatured TCR $\alpha$  and TCR $\beta$  chains, isolated from inclusion bodies. The refolded TCRs were purified further by size exclusion and ion exchange chromatography.

### **Surface plasmon resonance**

Equilibrium affinity and binding kinetics for TCRs binding to IA<sup>b</sup>-Padi4 and IA<sup>b</sup>-Add2 were obtained by surface plasmon resonance on a BIAcore 3000 instrument (BIAcore AB, Uppsala, Sweden). Measurements of Padi4-specific TCRs engaging IA<sup>b</sup>-Add2, and the Add2 TCR binding IA<sup>b</sup>-Padi4 were used as a negative control. pMHC complexes were coupled to the sensor surface via a biotin–streptavidin linkage, with the streptavidin amine coupled to a CM5 sensor chip. For equilibrium affinity experiments, ~2000–8000 resonance units (RU) of soluble biotinylated pMHC were captured on the chip surface by NeutrAvidin (Thermo Fisher). Experiments were performed at 25°C in 10 mM HEPES, 150 mM NaCl, 3 mM EDTA, and 0.005% surfactant P20 at pH 7.4. Soluble TCR was injected for 30–120 sec at a flow rate of 5 uL/min at concentrations ranging from 0.5 – 150 μM. Data points were collected at 0.4-s intervals and identical injections over a flow cell containing an irrelevant MHC-I complex were subtracted. The data were analyzed with BIAeval v4.1 and Prism v7.04 (GraphPad) software and equilibrium binding affinity ( $K_D$ ) was determined using a 1:1 Langmuir binding model. For kinetic experiments, 500–1000 RU of soluble pMHC was captured on the NeutrAvidin-coupled CM5 chip. TCRs were injected at a flow rate of 95 uL/min for 15–30 s with a dissociation time of 180 s between each sample. TCR concentrations ranged from 0.25 – 40 μM. Data points were collected at 0.2 s intervals and reference cell adjustments were made as described above. Kinetic data were analyzed with BiaEval software. The dissociation rate ( $k_{off}$ ) was determined by fitting the dissociation phase of the curve with a 1:1 Langmuir dissociation model. The half life ( $t_{1/2}$ ) and association rate ( $k_{on}$ ) were determined from the calculated  $K_D$  and  $k_d$  values. Values for the calculated confinement time,  $k_a$ , were done as described using a  $k_{on}$  rebinding threshold of 60,000 1/M\*s<sup>27</sup>.

### **Crystallization and data collection**

Soluble TCR and pMHC were mixed in a 1:1 ratio at equimolar concentrations of 10mg/ml in 10 mM Tris pH 7.5. Crystals of the 4699, 5287, and 4738 TCRs in complex with IA<sup>b</sup>-Padi4 were grown in 100 mM Sodium Cacodylate, 100 mM Sodium Citrate with 14% (w/v) PEG4000 pH 6.0 (4699), 14% (w/v) PEG4000 pH 5.6 (5287), or 12% (w/v) PEG4000 pH 5.8 (4738). Crystals of the 6235, 6236, and 6256 in complex with IA<sup>b</sup>-Padi4 were grown in 100 mM Sodium Cacodylate, 100 mM Sodium Citrate, 14% (w/v) PEG4000 pH 5.8. All crystals were grown at 25°C using hanging drop vapor diffusion. Crystals were cryopreserved by transferring to crystallization buffer containing 20% glycerol/80% mother liquor and flash frozen in liquid nitrogen. X-ray diffraction data were indexed, integrated, and scaled with XDS<sup>63</sup>. Unit cell parameters and data collection statistics are shown in Supplementary Table 2.

### **Structure determination**

Initial phases were obtained by molecular replacement using Phaser<sup>64</sup> using PDB 4P23 as the search model. One TCR and pMHC molecule per asymmetric unit were present in all six structures. Rigid body refinement followed by cycles of coordinate position, atomic displacement factor, and translation/libration/screw refinement were performed using PHENIX<sup>65</sup>, alternated with manual model adjustments in Coot<sup>66</sup>. Density for the peptide, TCR variable domains, and MHC was clearly observed in composite omit maps built by the Crystallography and NMR System<sup>67</sup>. No density was observed for the linker (GGGGSLVPRGSGGGGS) tethering the peptide to the N-terminal end of the MHC β chain. The structure was evaluated during refinement with MolProbity<sup>68</sup>.

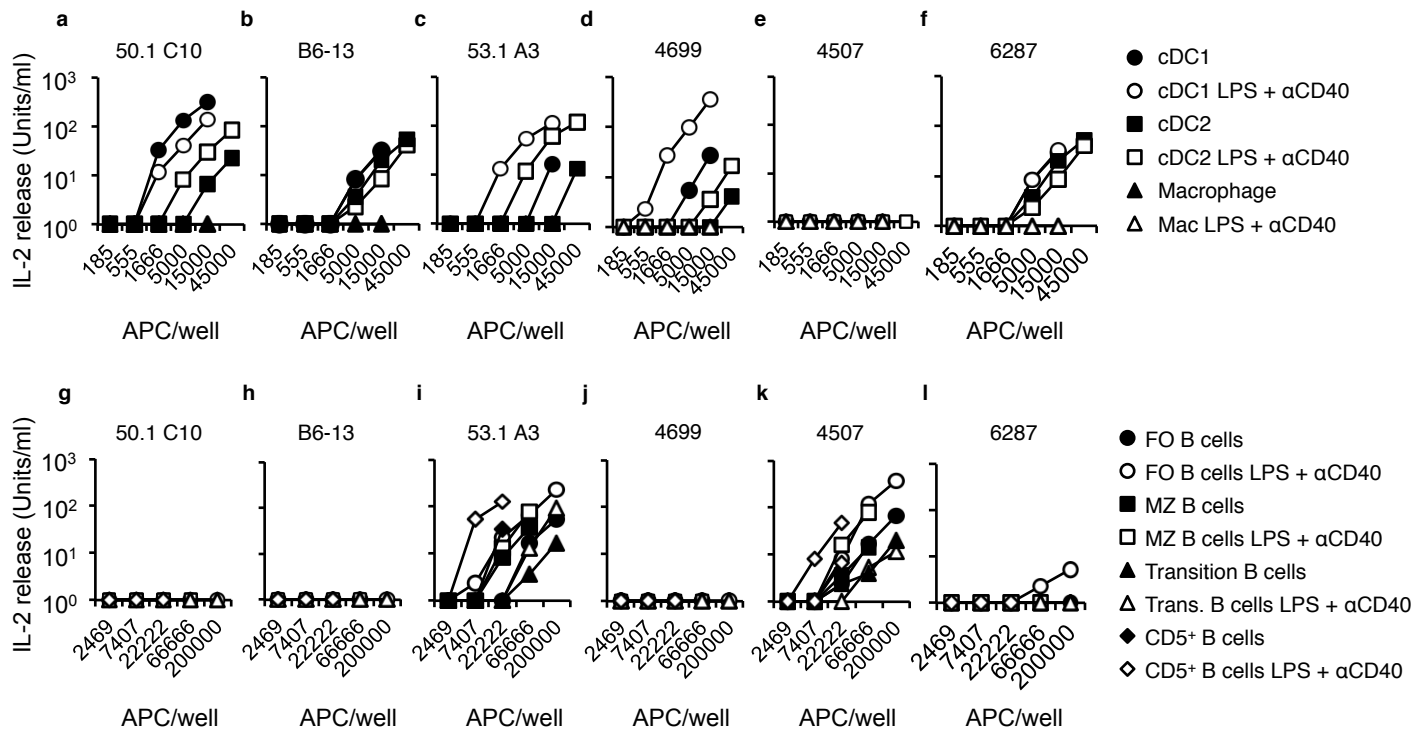
### **Structure analysis**

All six TCR:IA<sup>b</sup>-Padi4 complexes were superimposed in PyMOL (Delano Scientific) using the pair fit function, aligning the  $\alpha$  carbons of the MHC helices. Contacts were calculated using a 4Å cutoff in Ncont (CCP4 Suite). Buried Surface Area was determined by the PISA server from PDBe using a 1.4Å radius probe <sup>69</sup>. TCR crossing and incident angles were calculated as previously described <sup>70</sup>. PDB coordinates for other TCR:pMHC complexes used in crossing/incident angle and BSA calculations include: 1AO7, 1BD2, 1D9K, 1FOo, 1G6R, 1J8H, 1KJ2, 1LP9, 1MI5, 1MWA, 1NAM, 1OGA, 1QRN, 1QSE, 1QSF, 1U3H, 1YMM, 1ZGL, 2AK4, 2BNQ, 2BNR, 2E7L, 2F53, 2GJ6, 2IAM, 2IAN, 2NX5, 2OI9, 2OL3, 2P5E, 2P5W, 2PXY, 2VLR, 2WBJ, 2YPL, 2Z31, 3C5Z, 3C6o, 3C6L, 3DXA, 3E2H, 3E3Q, 3FFC, 3GSN, 3H9S, 3HG1, 3KPR, 3KPS, 3MBE, 3MV7, 3MV8, 3MV9, 3O4L, 3O6F, 3PL6, 3PQY, 3PWP, 3QDG, 3QDJ, 3QDM, 3QEQ, 3QFJ, 3QIB, 3QIU, 3QIW, 3RDT, 3RGV, 3SJV, 3TF7, 3TFK, 3TJH, 3TPU, 3UTT, 3VXM, 3VXR, 3VXS, 3VXU, 4E41, 4FTV, 4G8G, 4G9F, 4GG6, 4GRL, 4H1L, 4JFD, 4JFE, 4JFF, 4JRX, 4JRY, 4MAY, 4MJI, 4MNQ, 4MS8, 4MVB, 4MXQ, 4NoC, 4N5E, 4NHU, 4OZF, 4OZG, 4OZH, 4OZI, 4P23, 4P2O, 4P2Q, 4P2R, 4P46, 4P4K, 4P5T, 4PRH, 4PRI, 4PRP, 4QRP, 4Y19, 4Y1A, 4Z7U, 4Z7V, 4Z7W, 5BRZ, 5BSO, 5D2L, 5D2N, 5EU6, 5HHM, 5HHO, 5JZI. Electron density shown in Supplementary Fig. 6 was calculated from a 2Fobs-Fcalc map contoured to 1.5 sigma displayed in PyMOL.

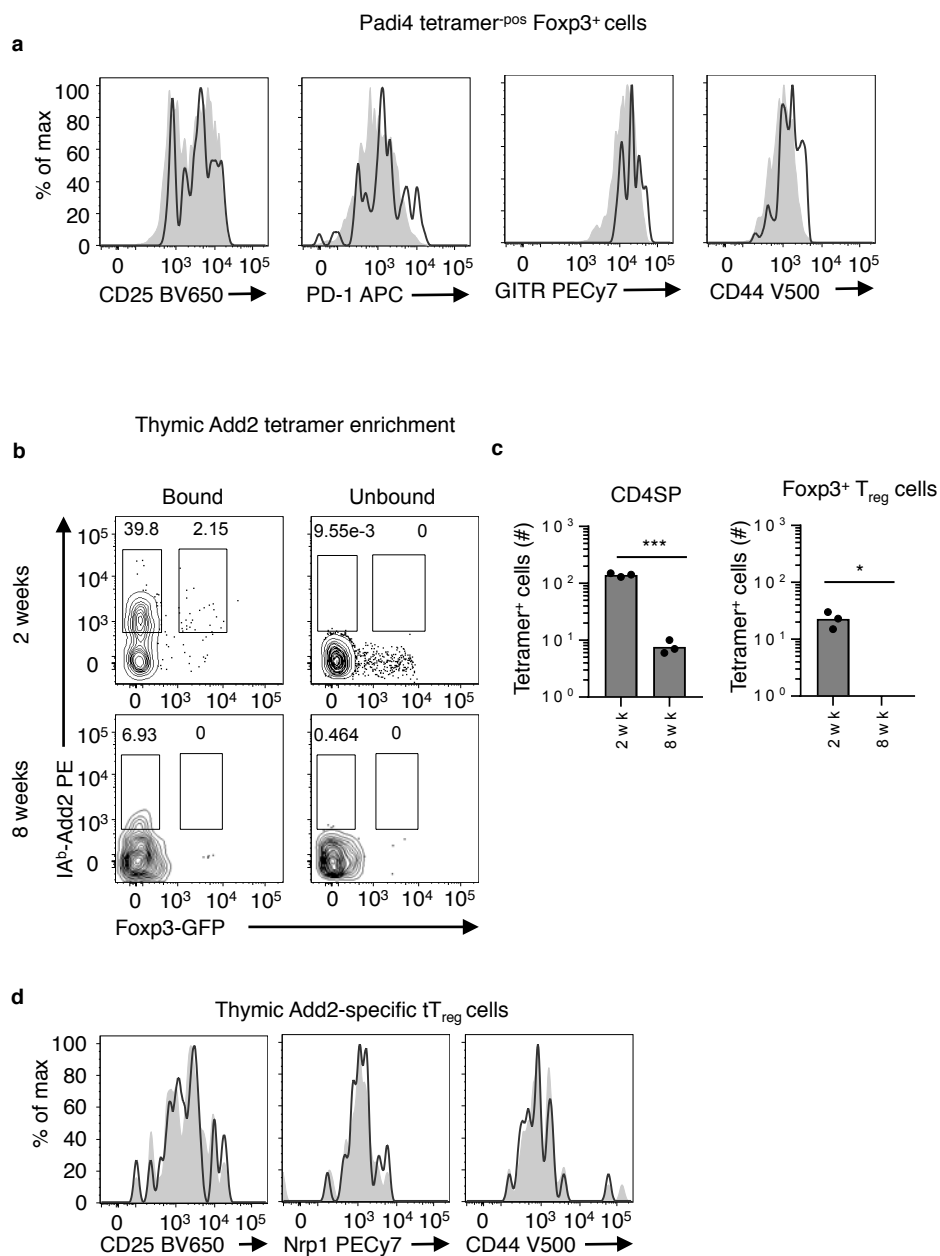
## Supplementary References

51. Gilligan DM, Lozovatsky L, Gwynn B, Brugnara C, Mohandas N, Peters LL. Targeted disruption of the beta adducin gene (*Add2*) causes red blood cell spherocytosis in mice. *Proc Natl Acad Sci U S A* 1999, **96**(19): 10717-10722.
52. Hemmers S, Teijaro JR, Arandjelovic S, Mowen KA. PAD4-mediated neutrophil extracellular trap formation is not required for immunity against influenza infection. *PLoS One* 2011, **6**(7): e22043.
53. Stadinski BD, Trenh P, Smith RL, Bautista B, Huseby PG, Li G, *et al.* A role for differential variable gene pairing in creating T cell receptors specific for unique major histocompatibility ligands. *Immunity* 2011, **35**(5): 694-704.
54. Moon JJ, Chu HH, Hataye J, Pagan AJ, Pepper M, McLachlan JB, *et al.* Tracking epitope-specific T cells. *Nat Protoc* 2009, **4**(4): 565-581.
55. Bogunovic B, Srinivasan P, Ueda Y, Tomita Y, Maric M. Comparative quantitative mass spectrometry analysis of MHC class II-associated peptides reveals a role of GILT in formation of self-peptide repertoire. *PLoS One* 2010, **5**(5): e10599.
56. Bozzacco L, Yu H, Zebroski HA, Dengjel J, Deng H, Mojsov S, *et al.* Mass spectrometry analysis and quantitation of peptides presented on the MHC II molecules of mouse spleen dendritic cells. *Journal of proteome research* 2011, **10**(11): 5016-5030.
57. Dongre AR, Kovats S, deRoos P, McCormack AL, Nakagawa T, Paharkova-Vatchkova V, *et al.* In vivo MHC class II presentation of cytosolic proteins revealed by rapid automated tandem mass spectrometry and functional analyses. *Eur J Immunol* 2001, **31**(5): 1485-1494.
58. Sofron A, Ritz D, Neri D, Fugmann T. High-resolution analysis of the murine MHC class II immunopeptidome. *Eur J Immunol* 2016, **46**(2): 319-328.
59. Fugmann T, Sofron A, Ritz D, Bootz F, Neri D. The MHC Class II Immunopeptidome of Lymph Nodes in Health and in Chemically Induced Colitis. *J Immunol* 2017, **198**(3): 1357-1364.
60. Nanaware PP, Jurewicz MM, Leszyk J, Shaffer SA, Stern LJ. HLA-DO modulates the diversity of the MHC-II self-peptidome. *Mol Cell Proteomics* 2018.
61. Rudensky A, Preston-Hurlburt P, al-Ramadi BK, Rothbard J, Janeway CA, Jr. Truncation variants of peptides isolated from MHC class II molecules suggest sequence motifs. *Nature* 1992, **359**(6394): 429-431.
62. Yang X, Liu D, Lv N, Zhao F, Liu F, Zou J, *et al.* TCRklass: a new K-string-based algorithm for human and mouse TCR repertoire characterization. *J Immunol* 2015, **194**(1): 446-454.
63. Kabsch W. Xds. *Acta Crystallogr D Biol Crystallogr* 2010, **66**(Pt 2): 125-132.

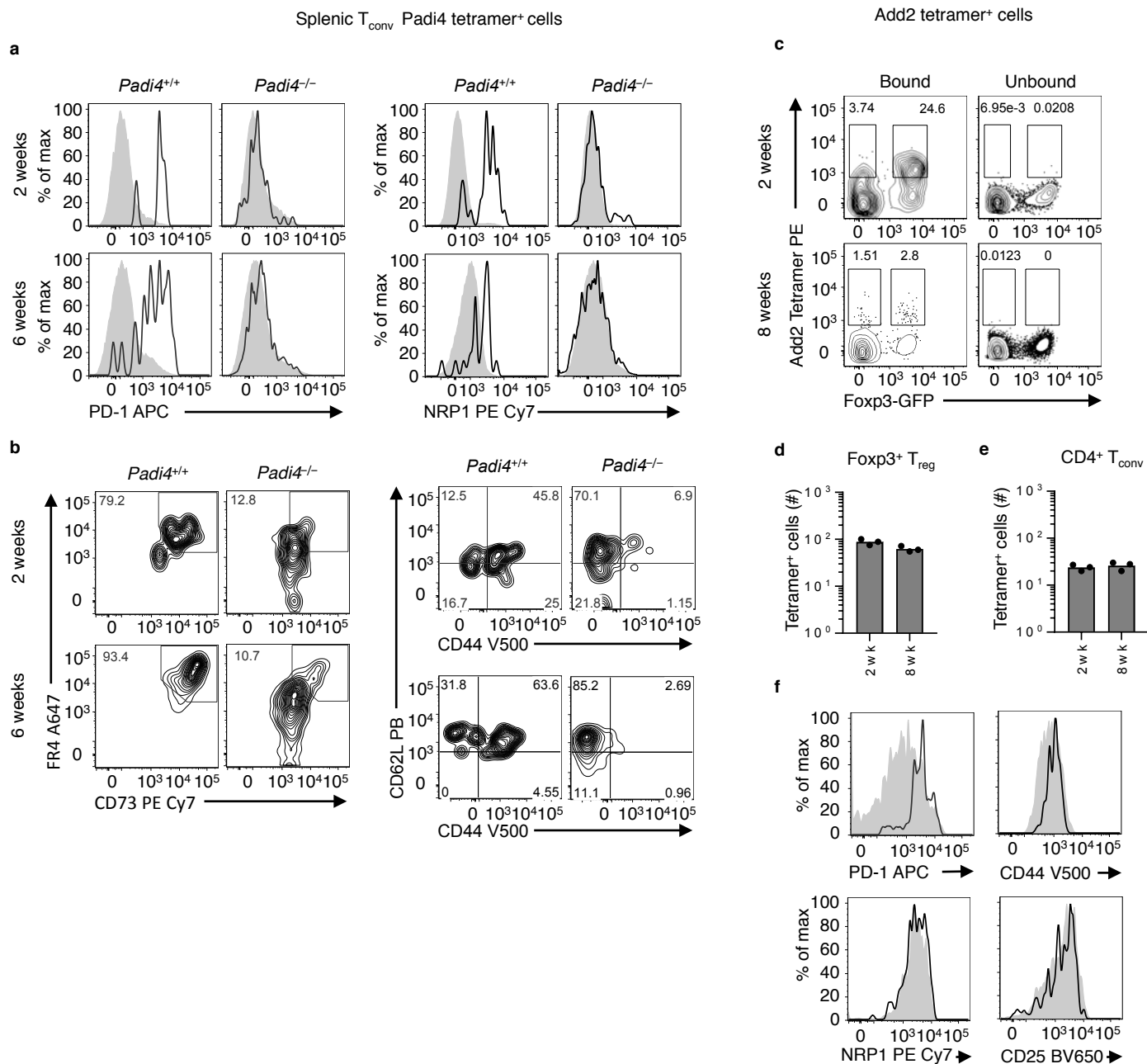
64. McCoy AJ, Grosse-Kunstleve RW, Adams PD, Winn MD, Storoni LC, Read RJ. Phaser crystallographic software. *J Appl Crystallogr* 2007, **40**(Pt 4): 658-674.
65. Adams PD, Afonine PV, Bunkoczi G, Chen VB, Davis IW, Echols N, *et al.* PHENIX: a comprehensive Python-based system for macromolecular structure solution. *Acta Crystallogr D Biol Crystallogr* 2010, **66**(Pt 2): 213-221.
66. Emsley P, Cowtan K. Coot: model-building tools for molecular graphics. *Acta Crystallogr D Biol Crystallogr* 2004, **60**(Pt 12 Pt 1): 2126-2132.
67. Brunger AT. Version 1.2 of the Crystallography and NMR system. *Nat Protoc* 2007, **2**(11): 2728-2733.
68. Williams CJ, Headd JJ, Moriarty NW, Prisant MG, Videau LL, Deis LN, *et al.* MolProbity: More and better reference data for improved all-atom structure validation. *Protein science : a publication of the Protein Society* 2018, **27**(1): 293-315.
69. Krissinel E, Henrick K. Inference of macromolecular assemblies from crystalline state. *J Mol Biol* 2007, **372**(3): 774-797.
70. Rudolph MG, Stanfield RL, Wilson IA. How TCRs bind MHCs, peptides, and coreceptors. *Annu Rev Immunol* 2006, **24**: 419-466.



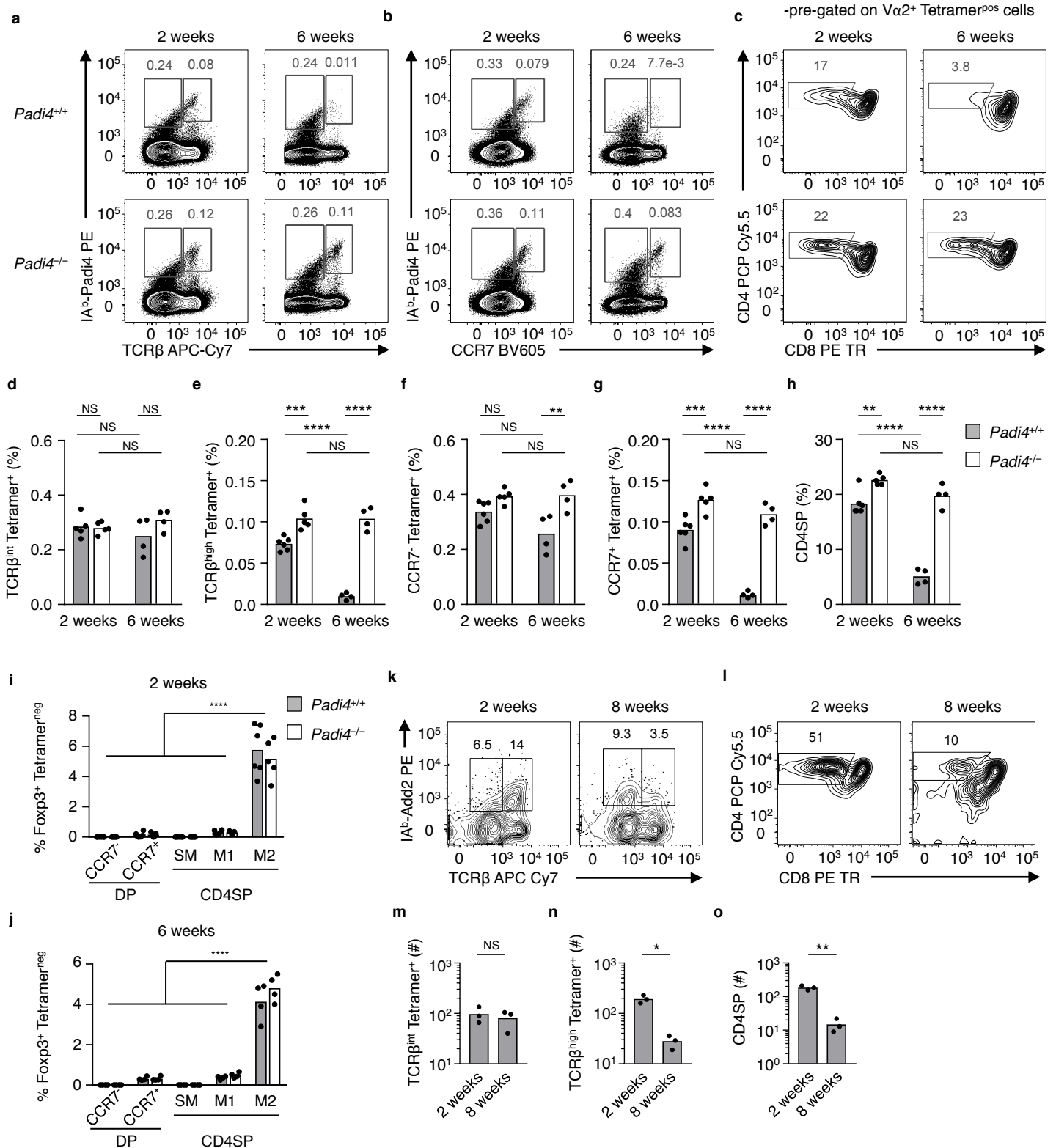
**Supplementary Figure 1.** T cell receptors expressed on neonate-derived  $tT_{reg}$  cells can recognize steady state and inflammation-dependent self-antigens presented by dendritic cell and/or B cell subsets. **(a)** IL-2 response of B6-50.1C10, **(b)** B6-13 **(c)** 53.1.A3, **(d)** 4699, **(e)** 4507 **(f)** 4699 **(g)** 4783  $tT_{reg}$  hybridomas cultured with titrating amounts of cDC1, cDC2 and macrophages or **(g-l)** B cell subsets isolated from naïve mice (filled symbol) or mice pretreated with LPS and  $\alpha$ CD40 (open symbol). Results are from three independent experiments with similar results.



**Supplementary Figure 2.** Phenotype and age-dependent selection of Padi4- and Add2-specific tT<sub>reg</sub> cells in the thymus of YAe62β.Foxp3-GFP mice. **(a)** Flow cytometry analyzing the expression of CD25, PD-1, GITR and CD44 on IA<sup>b</sup>-Padi4 tetramer<sup>pos</sup> Va2<sup>+</sup>CD4<sup>+</sup> tT<sub>reg</sub> cells in thymus of YAe62β.Foxp3-GFP at 2 weeks of age (black line). Gray histograms are IA<sup>b</sup>-Padi4 tetramer<sup>neg</sup> Va2<sup>+</sup>CD4<sup>+</sup> tT<sub>reg</sub> cells in the same mice. Data are example from three independent experiments giving similar results. **(b)** Age-dependent thymic development of Add2<sub>606-621</sub>-specific tT<sub>reg</sub> cells. Flow cytometry of Va2<sup>+</sup> CD4SP thymocytes in YAe62β.Foxp3-GFP mice at 2 weeks (top row) and 8 weeks of age (bottom row) following tetramer-based enrichment, stained with IA<sup>b</sup>-Add2 tetramer. **(c)** Quantification of IA<sup>b</sup>-Add2 tetramer<sup>pos</sup> Va2<sup>+</sup> Foxp3-GFP<sup>neg</sup> CD4SP and Foxp3-GFP<sup>pos</sup> Va2<sup>+</sup> CD4SP thymocytes in YAe62β.Foxp3-GFP mice at different ages. **(d)** Flow cytometry analyzing the expression of CD25, NRP1, and CD44 on IA<sup>b</sup>-Add2 tetramer<sup>pos</sup> Va2<sup>+</sup>CD4<sup>+</sup>CD8<sup>-</sup>Foxp3-GFP<sup>pos</sup> thymocytes in YAe62β.Foxp3-Gfp mice at 2 weeks of age (black line). (b-d) Data are from three independent experiments with similar results, bars represent the mean cell number. Gray is expression on Foxp3<sup>+</sup> tetramer negative cells in the same mice. (c) CD4SP \*\*\*P<0.001 unpaired 2-tailed t test; Foxp3<sup>+</sup> T<sub>reg</sub> cells \*P<0.05 unpaired 2-tailed t test with Welch's correction.

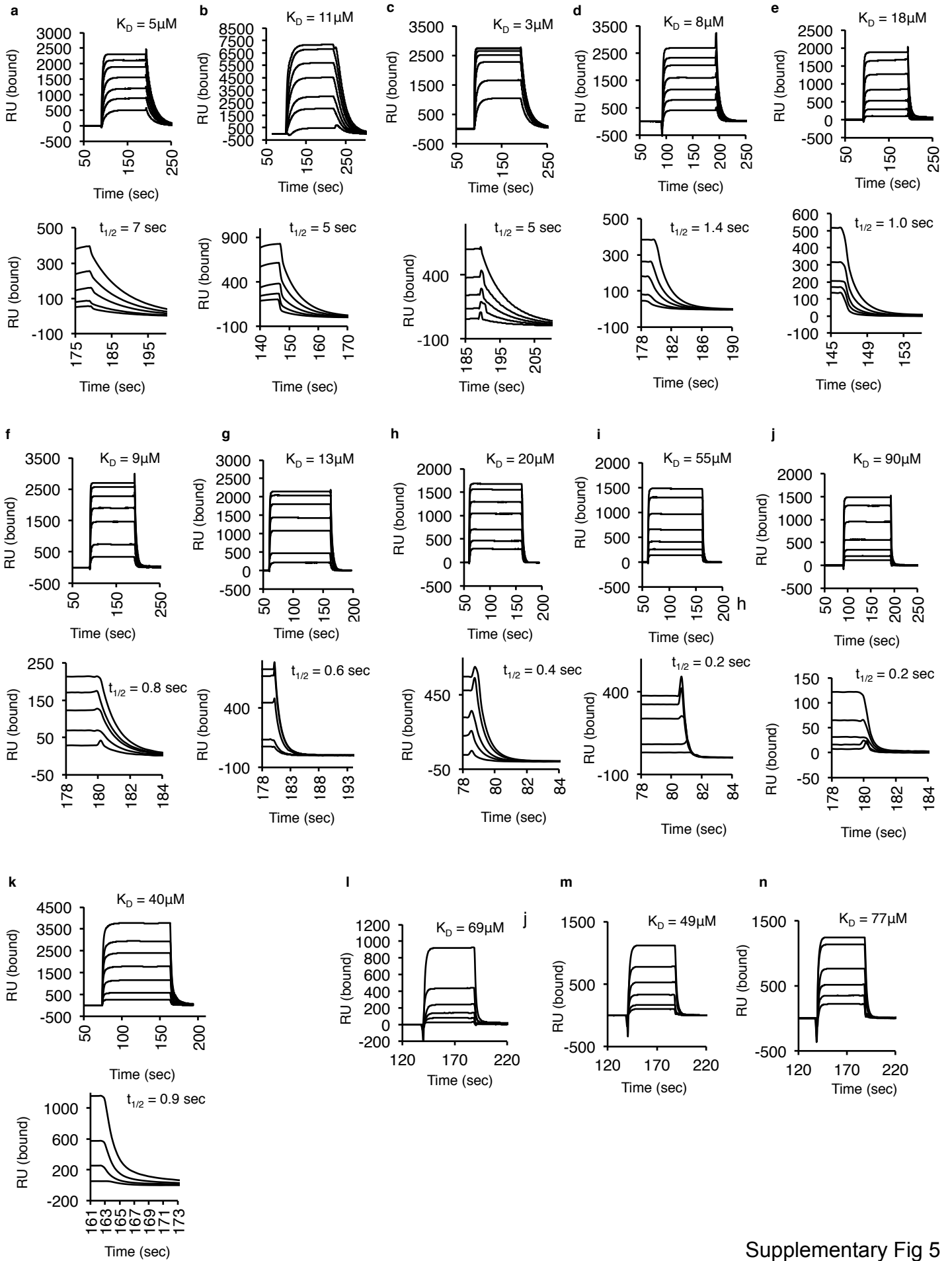


**Supplementary Figure 3.** Phenotype of splenic Padi4-specific CD4<sup>+</sup> T<sub>conv</sub> cells and Add2-specific tT<sub>reg</sub> cells. Padi4<sub>92-105</sub>-specific CD4<sup>+</sup> T cells have a naïve phenotype in *Padi4*<sup>-/-</sup> mice. **(a)** Flow cytometry of IA<sup>b</sup>-Padi4 tetramer<sup>pos</sup> Fcγ2b-GFP<sup>neg</sup> Vα2<sup>+</sup> CD4 T cells in *Padi4*<sup>+/+</sup> and *Padi4*<sup>-/-</sup> YAe62β.*Foxp3-Gfp* mice at 2 weeks (top row) and 6 weeks of age (bottom row) for PD-1 and Nrp1 (black line), and **(b)** FR4 and CD73, and CD44 and CD62L. Frequency and total cell numbers are shown in Fig. 4. **(c)** Flow cytometry of Vα2<sup>+</sup> CD4<sup>+</sup> T cells in YAe62β.*Foxp3-Gfp* mice at 2 weeks (top row) and 8 weeks of age (bottom row) following tetramer enrichment protocol, stained with IA<sup>b</sup>-Add2 tetramer. Quantification of IA<sup>b</sup>-Add2 tetramer<sup>pos</sup> **(d)** Vα2<sup>+</sup> Fcγ2b-GFP<sup>pos</sup> tT<sub>reg</sub> cells and **(e)** Vα2<sup>+</sup> Fcγ2b-GFP<sup>neg</sup> CD4 T<sub>conv</sub> cells in YAe62β.*Foxp3-GFP* mice at 2 and 8 weeks age. **(f)** Flow cytometry analyzing the expression of PD-1, CD44, Nrp1 and CD25 on Vα2<sup>+</sup> CD4<sup>+</sup> Fcγ2b-GFP<sup>+</sup> T<sub>reg</sub> cells isolated from 2 week old YAe62β.*Foxp3-GFP* mice (black line). Gray histograms are IA<sup>b</sup>-Add2 tetramer<sup>neg</sup> Vα2<sup>+</sup> CD4<sup>+</sup> Fcγ2b-GFP<sup>pos</sup> T<sub>reg</sub> cells in the same mice. (a-f) Data from 3 independent experiments with similar results with 3 mice per group, bars represent the data mean. (d, e) NS P>0.05 ratio unpaired 2-tailed t test.



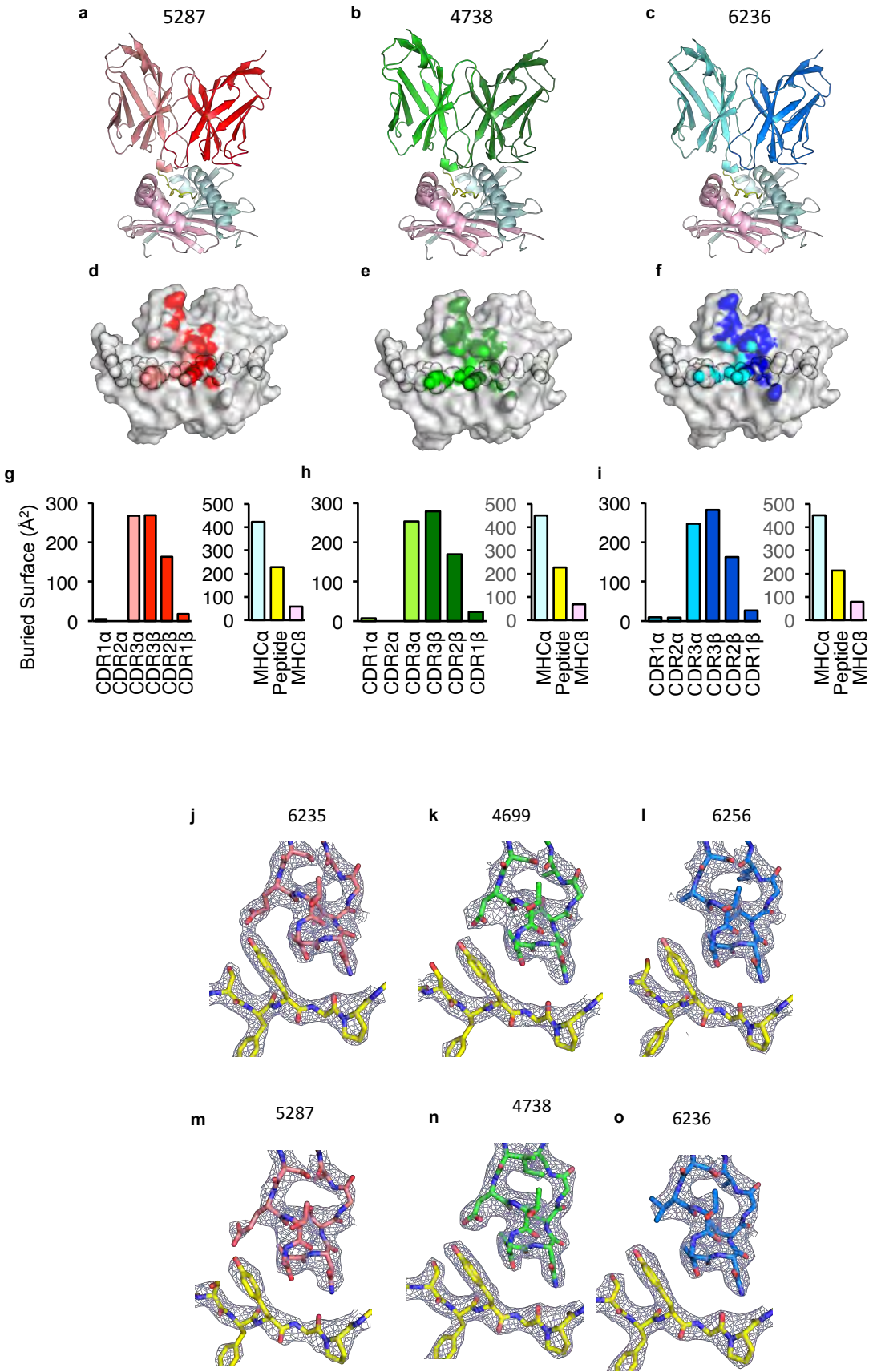
**Supplementary Figure 4.** Padi4<sup>-</sup> and Add2-specific thymocytes undergo negative selection at the DP to CD4SP transition in adult thymus. **(a-h)** The neonate but not adult thymus generates Padi4-tetramer<sup>pos</sup> TCRβ<sup>hi</sup>, CCR7<sup>+</sup> CD4SP thymocytes. **(a,b)** Flow cytometry analyses of total Va2<sup>+</sup> thymocyte isolated from neonate and adult, *Padi4*<sup>+/+</sup> (top row) and *Padi4*<sup>-/-</sup> (bottom row) YAe62β.*Foxp3-GFP* mice, for IA<sup>b</sup>-Padi4 tetramer binding and **(a)** TCRβ and **(b)** CCR7 expression. **(c)** Flow cytometry analyses of total Va2<sup>+</sup> IA<sup>b</sup>-Padi4 tetramer<sup>pos</sup> thymocytes for CD4 and CD8 expression. **(d-h)** Quantification of the frequency of Va2<sup>+</sup> IA<sup>b</sup>-Padi4 tetramer<sup>pos</sup> thymocytes in neonatal and adult thymus that are **(d)** TCRβ<sup>int</sup>, **(e)** TCRβ<sup>hi</sup>, **(f)** CCR7<sup>neg</sup>, **(g)** CCR7<sup>+</sup> and **(h)** CD4SP. **(i,j)** Quantification of total t<sub>reg</sub> development in **(i)** neonate and **(j)** adult thymus,

**Supplementary Figure 4 cont.** based on thymocytes stage of development. Data are derived from 3 independent experiments giving similar results, bars represent the data mean; n = 6 WT and *Padi4*<sup>-/-</sup> mice at 2 at weeks old and n = 4 at 6 weeks old. **(k)** Flow cytometry analyses of total Vα2<sup>+</sup> thymocyte isolated from neonate and adult, YAe62β.*Foxp3-GFP* following IA<sup>b</sup>-Add2 tetramer enrichment, for IA<sup>b</sup>-Add2 tetramer binding and TCRβ expression. **(l)** Flow cytometry analyses of total Vα2<sup>+</sup> IA<sup>b</sup>-Add2 tetramer<sup>pos</sup> thymocytes for CD4 and CD8 expression. **(m-o)** Quantification of frequency of Vα2<sup>+</sup> IA<sup>b</sup>-Add2 tetramer<sup>pos</sup> thymocytes in neonatal and adult thymus that are **(m)** TCRβ<sup>int</sup>, **(n)** TCRβ<sup>hi</sup> and **(o)** CD4SP. Data pooled from 3 independent experiments giving similar results with 3 mice per group, bars represent the data mean. (d-j) Significance identified using a one-way ANOVA Sidak's multiple comparison test and (m,o) unpaired 2-tailed t test. ns P>0.05, \*P<0.05, \*\*P<0.01, \*\*\*P<0.001, \*\*\*\*P<0.0001.

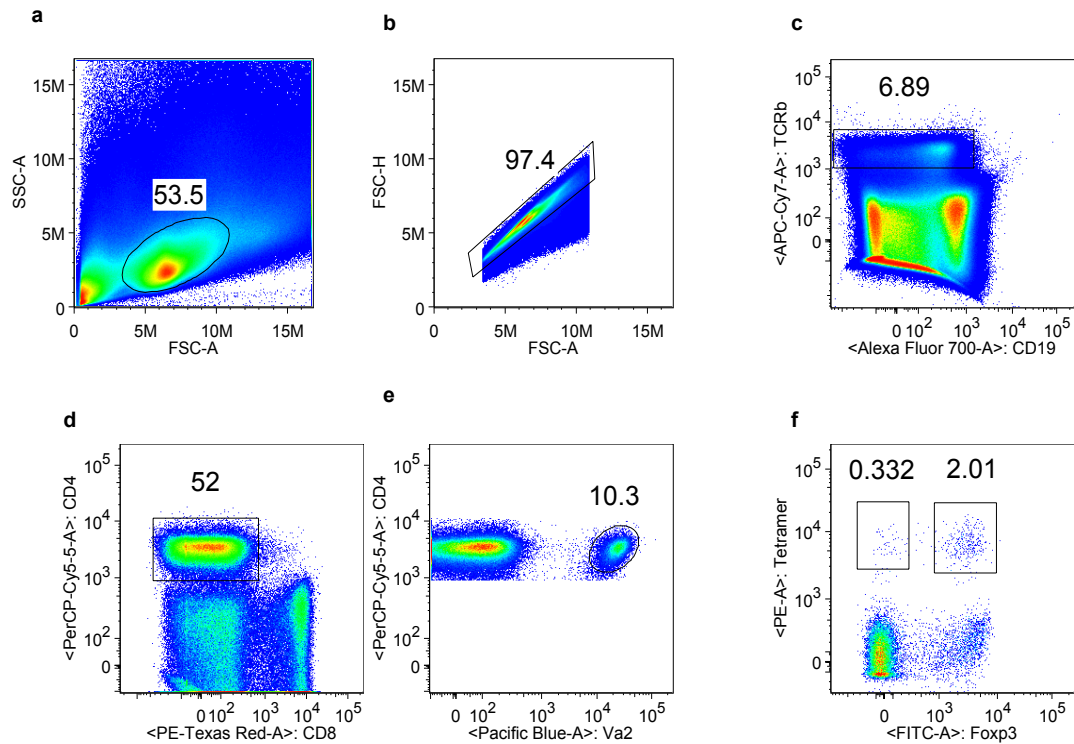


Supplementary Fig 5

**Supplementary Figure 5.** Surface plasmon resonance sensograms to measure the equilibrium affinity and kinetics of TCRs binding IA<sup>b</sup>-Padi4 and Add2. **(a-j)** Surface plasmon resonance sensograms of 0.5-150μM soluble **(a)** 5287, **(b)** 5290, **(c)** 6235, **(d)** 4699, **(e)** 4738 **(f)** 6239, **(g)** 6236, **(h)** 6256, **(i)** 6237 and **(j)** 6238 TCRs binding IA<sup>b</sup>-Padi4; equilibrium affinity (top row) and binding kinetics (bottom row). **(k)** Surface plasmon resonance sensograms of 1-150μM soluble 6287 TCR binding IA<sup>b</sup>-Add2; equilibrium affinity (top row) and binding kinetics (bottom row). **(l-n)** Surface plasmon resonance sensograms of 5-150μM soluble **(i)** 6235, **(j)** 4699 and **(k)** 6256 TCRs binding IA<sup>b</sup>-Padi4 P2F. Disassociation sensograms for determining  $t_{1/2}$  are shown in Fig. 8. Sensograms are background subtracted from each TCR interacting with a non-cognate (IA<sup>b</sup>-Add2 or IA<sup>b</sup>-Padi4 ligand). Data are examples of 4 biological replicates, giving similar results.



**Supplementary Figure 6.** Padi4-specific TCRs with long, moderate and short dwell times use conventional docking orientations on IA<sup>b</sup>-Padi4. **(a-c)** Ribbon diagrams of **(a)** 5287 (pdb: 6MKR), **(b)** 4378 (pdb: 6MNG) and **(c)** 6236 (pdb: 6MNN) TCRs binding IA<sup>b</sup>-Padi4. The 5287 TCR is colored red (TCR $\beta$ ) and pink (TCR $\alpha$ ); the 4378 TCR is colored dark green (TCR $\beta$ ) and light green (TCR $\alpha$ ); the 6236 TCR is colored dark blue (TCR $\beta$ ) and light blue (TCR $\alpha$ ). IA<sup>b</sup>-Padi4 is colored cyan (IA<sup>b</sup> $\alpha$  chain), yellow (peptide), and magenta (IA<sup>b</sup> $\beta$  chain). **(d-f)** Projections of the **(d)** 5287, **(e)** 4378 and **(f)** 6236 TCRs bound to IA<sup>b</sup>-Padi4. 5287 TCR $\alpha$  contacts are colored pink, TCR $\beta$  contacts are colored red; 4378 TCR $\alpha$  contacts are colored light green, TCR $\beta$  contacts are colored dark green; 6236 TCR $\alpha$  contacts are colored light blue, TCR $\beta$  contacts are colored dark blue. The peptide residues are outlined in black. **(g-i)** The amount of buried surface area (BSA) of the **(g)** 5287:IA<sup>b</sup>-Padi4, **(h)** 4378:IA<sup>b</sup>-Padi4 and **(i)** 6236:IA<sup>b</sup>-Padi4 complexes contributed by TCR $\alpha$  and TCR $\beta$  loops, and the peptide or MHC chains. Figures were made with PyMol. **(j-o)** Electron density in the **(j)** 6235, **(k)** 4699, **(l)** 6256, **(m)** 5287, **(n)** 4783 and **(o)** 6236 CDR3 $\alpha$  and peptide region contoured at 1.5 sigma from I2Fobs-Fcalcl map with phases calculated for a model with peptide p2Y (yellow).



**Supplementary Figure 7.** Gating strategy to analyze Padi4-specific  $tT_{reg}$  cells and  $CD4^+$   $T_{conv}$  cells in 2 week old YA $\alpha 62\beta$  mice. (a) Lymphocytes were gated on forward and side scatter and (b) doublets removed by gating FSC-H by FSC-A. (c) TCR $^+$  lymphocytes were then (d) gated for the expression of (d)  $CD4^+$  and  $CD8^{neg}$ , and (e) the expression of Va2. (f) Gated T cells were then analyzed for Foxp3-GFP expression, and staining with IA $^b$ -Padi4 tetramer. Subsequent phenotypic stains were then analyzed on these populations.

Supplementary Table 1. Neonatal tT<sub>reg</sub> TCR sequences and identified self-peptide ligand reactivity

Clone ID	TCRβ	Vβ	CDR3β	Jβ	TCRα	Vα	CDR3α	Jα	Antigen (gene)	Region	Peptide	EC <sub>50</sub> (nM)
4699	8	TRBV13-2	CASGDFWGD TLYFG	TRBJ2-4	2	TRAV14D-3/DV8	CAASDTGANTGKLT F	TRAJ52	<i>Padi4</i>	92-105	VRVSYGPKTSPVQ	0.814
4738	8	TRBV13-2	CASGDFWGD TLYFG	TRBJ2-4	2	TRAV14D-3/DV8	CAGIDTGANTGKLT F	TRAJ52	<i>Padi4</i>	92-105	VRVSYGPKTSPVQ	2.29
6287	8	TRBV13-2	CASGDFWGD TLYFG	TRBJ2-4	2	TRAV14-2	CAARATGGNNKLT F	TRAJ56	<i>Add2</i>	606-621	SPSKAGTKSPAVSPSK	7.26
5853	8	TRBV13-2	CASGDFWGD TLYFG	TRBJ2-4	11	TRAV4D-4	CASRNSNNRIFF	TRAJ31	<i>Gpd2</i>	235-250	TAARYGAATAN YMEVV	35.2
5803	8	TRBV13-2	CASGDFWGD TLYFG	TRBJ2-4	8	TRAV12D-1	CALRNTGNYKYVF	TRAJ40	<i>Gpd2</i>	235-250	TAARYGAATAN YMEVV	79.6
5915	8	TRBV13-2	CASGDFWGD TLYFG	TRBJ2-4	11	TRAV4D-3	CAARGGNTGKLIF	TRAJ37	<i>Gpd2</i>	235-250	TAARYGAATAN YMEVV	110
4630	8	TRBV13-2	CASGDFWGD TLYFG	TRBJ2-4	2	TRAV14-2	CAASENSGTYQRF	TRAJ13	<i>Gsn</i>	599-614	AAYLWVGAGASEA EKT	80.4
4513	8	TRBV13-2	CASGDFWGD TLYFG	TRBJ2-4	8	TRAV12-3	CALSALNNNAPRF	TRAJ43	<i>Kcnk5</i>	290-304	APKDSYQTSEVFINQ	100
4748	8	TRBV13-2	CASGDFWGD TLYFG	TRBJ2-4	2	TRAV14-2	CAAANS GTYQRF	TRAJ13	<i>Rps25</i>	62-76	VPNYKLITPAVV SER	164
4754	8	TRBV13-2	CASGDFWGD TLYFG	TRBJ2-4	2	TRAV14-2	CAASEGN NRIFF	TRAJ31	<i>Hist1h1c</i>	155-171	PKKAKKPAAA AVTKKVA	189
52.1 A6	11	TRBV16	CASSFDRGQAPLF	TRBJ1-5	2	TRAV12-2	CAASPSSGQKLVF	TRAJ16	<i>Cltb</i>	40-53	NDPGFGAPAASQVA	191
4776	8	TRBV13-2	CASGDFWGD TLYFG	TRBJ2-4	2	TRAV14-2	CAASRAGSGGKLT L	TRAJ44	<i>Ppp1cb</i>	311-327	SGRPVTPPR TANPPKRR	294
4623	8	TRBV13-2	CASGDFWGD TLYFG	TRBJ2-4	2	TRAV14-1	CAAIANTGANTGKLT F	TRAJ52	<i>Galnt4</i>	29-44	VSTLYASPGAGGAREL	336
4753	8	TRBV13-2	CASGDFWGD TLYFG	TRBJ2-4	2	TRAV14-1	CAASANTGANTGKLT F	TRAJ52	<i>Galnt4</i>	29-44	VSTLYASPGAGGAREL	343
50.1 C10	8	TRBV13-2	CASGDGLGGDTQYF	TRBJ2-5	11	TRAV4D-4	CAATGTGGYKVVF	TRAJ12	<i>Cilp</i>	1128-1142	SAFYQLQSTPARSPA	347
3H14	8	TRBV13-2	CASGDFWGD TLYFG	TRBJ2-4	2	TRAV14D-3/DV8	CAAVATGGNNKLT F	TRAJ56	<i>Ugcg</i>	233-247	IAEDYFMAKAIADRG	59.7
4819	8	TRBV13-2	CASGDFWGD TLYFG	TRBJ2-4	2	TRAV14-2	CAASETGANTGKLT F	TRAJ52	<i>Ugcg</i>	233-247	IAEDYFMAKAIADRG	372
4820	8	TRBV13-2	CASGDFWGD TLYFG	TRBJ2-4	2	TRAV14-2	CAASITGSGGKLT L	TRAJ44	<i>Ugcg</i>	233-247	IAEDYFMAKAIADRG	752
4751	8	TRBV13-2	CASGDFWGD TLYFG	TRBJ2-4	2	TRAV14D-3/DV8	CAASRTGGNNKLT F	TRAJ56	<i>Ugcg</i>	233-247	IAEDYFMAKAIADRG	752
4787	8	TRBV13-2	CASGDFWGD TLYFG	TRBJ2-4	2	TRAV14D-3/DV8	CAASARVATGGNNKLT F	TRAJ56	<i>Map4k1</i>	385-400	DGSLKLVTP EGAPAPG	695
4777	8	TRBV13-2	CASGDFWGD TLYFG	TRBJ2-4	2	TRAV14-2	CAASGGADRLTF	TRAJ45	<i>Cmip</i>	160-174	KKIKYKVKVLSNPSR	695
4693	8	TRBV13-2	CASGDFWGD TLYFG	TRBJ2-4	8	TRAV12-3	CALSDRTNAYKVIF	TRAJ30	<i>Eif3f</i>	37-50	APTPAATPAASPAP	695
4507	8	TRBV13-2	CASGDFWGD TLYFG	TRBJ2-4	8	TRAV12-3	CALSDRTNTNKVVF	TRAJ34	<i>Aldh8a1</i>	50-65	EAAREAFP AWSSRS PQ	853
4731	8	TRBV13-2	CASGDFWGD TLYFG	TRBJ2-4	2	TRAV14D-3/DV8	CAASGGNYNQGKLIF	TRAJ23	<i>Ldha</i>	68-82	GSLFLKTPKIVSSKD	1150

TCR V and J regions defined using IMGT nomenclature.  
EC<sub>50</sub> values are average of 3 independent experiments.

**Supplementary Table 2. T cell response, affinity and kinetics of binding of Padi4 and Add2 specific TCRs**

TCR	Specificity	TRAV	CDR3a	IL2 release EC <sub>50</sub> (nM)	K <sub>D</sub> ( $\mu$ M)	k <sub>on</sub> (1/M·s) x 10 <sup>3</sup>	t <sub>1/2</sub> (s)	t <sub>a</sub> (s)
5287	Padi4 <sub>92-105</sub>	14-3	CAASETGANTGKLTF	0.02 ± 0.07	5 ± 0.4	20 ± 2	7 ± 0.2	8 ± 0.3
6235	Padi4 <sub>92-105</sub>	14D-3	CAASETGANTGKLTF	0.02 ± 0.03	3 ± 1.6	69 ± 30	5 ± 0.3	8 ± 3
5290	Padi4 <sub>92-105</sub>	14-2	CAAENTGANTGKLTF	0.02 ± 0.03	11 ± 0.5	15 ± 2	5 ± 0.2	6 ± 0.2
4699	Padi4 <sub>92-105</sub>	14D-3	CAASDTGANTGKLTF	0.6 ± 0.1	8 ± 2	62 ± 5	1.4 ± 0.1	2.3 ± 0.2
4738	Padi4 <sub>92-105</sub>	14D-3	CAGIDTGANTGKLTF	1.3 ± 0.2	18 ± 1	38 ± 10	1 ± 0.2	1.4 ± 0.2
6239	Padi4 <sub>92-105</sub>	14D-3	CAASNTGANTGKLTF	0.7 ± 0.1	9 ± 1	91 ± 14	0.8 ± 0.1	1.5 ± 0.2
6236	Padi4 <sub>92-105</sub>	14D-3	CAASVTGANTGKLTF	5 ± 1	13 ± 3	77 ± 18	0.6 ± 0.1	1.0 ± 0.2
6256	Padi4 <sub>92-105</sub>	14D-3	CAASATGANTGKLTF	41 ± 12	20 ± 2	91 ± 29	0.4 ± 0.1	0.8 ± 0.2
6237	Padi4 <sub>92-105</sub>	14D-3	CAASSTGANTGKLTF	1450 ± 120	55 ± 16	58 ± 21	0.2 ± 0.1	0.3 ± 0.1
6238	Padi4 <sub>92-105</sub>	14D-3	CAASTTGANTGKLTF	290 ± 40	90 ± 21	35 ± 12	0.2 ± 0.1	0.3 ± 0.1
6287	Add2 <sub>606-621</sub>	14-2	CAARATGGNNKLTF	40 ± 5	40 ± 20	20 ± 10	0.9 ± 0.1	1.2 ± 0.2
6235	Padi4 P2F	14D-3	CAASETGANTGKLTF	n/d	69 ± 6	70 ± 35	0.2 ± 0.05	0.3 ± 0.1
4699	Padi4 P2F	14D-3	CAASDTGANTGKLTF	n/d	49 ± 2	96 ± 48	0.2 ± 0.05	0.4 ± 0.2
6256	Padi4 P2F	14D-3	CAASATGANTGKLTF	n/d	77 ± 42	76 ± 37	0.2 ± 0.05	0.4 ± 0.2

The equilibrium affinities and kinetics of binding were determined by SPR measured in 4 four independent experiments. k<sub>on</sub> values were estimated from the measured K<sub>D</sub> and t<sub>1/2</sub> values. The standard error reported for IL2 release, K<sub>D</sub> and t<sub>1/2</sub> is based on one standard deviation. The error reported for the k<sub>on</sub> represents the maximum error associated with both the K<sub>D</sub> and t<sub>1/2</sub> values. The confinement time (t<sub>a</sub>) values were estimated from the average values of the k<sub>on</sub> and t<sub>1/2</sub>, using threshold for rebinding of 100,000 1/M·s. Reported t<sub>a</sub> error was calculated from the error associated with k<sub>on</sub>.

**Supplementary Table 3. Data collection and refinement statistics for TCRs in complex with I-Ab/padi4**

	<b>4699 :</b> <b>IA<sup>b</sup>-padi4</b>	<b>6235 :</b> <b>IA<sup>b</sup>-padi4</b>	<b>6256 :</b> <b>IA<sup>b</sup>-padi4</b>	<b>4738 :</b> <b>IA<sup>b</sup>-padi4</b>	<b>6236 :</b> <b>IA<sup>b</sup>-padi4</b>	<b>5287 :</b> <b>IA<sup>b</sup>-padi4</b>
<b>Data collection</b>						
Space group	C 1 2 1	C 1 2 1	C 1 2 1	C 1 2 1	C 1 2 1	C 1 2 1
Cell dimensions a,b,c (Å)	255.448, 73.643, 64.566	250.057, 69.03, 64.687	254.351, 73.771, 63.142	250.917 69.163 64.15	250.412 68.872 64.466	257.022, 73.761, 65.207
$\alpha,\beta,\gamma(^{\circ})$	90, 90.391, 90	90, 91.51, 90	90, 90.517, 90	90 91.479 90	90 91.97 90	90, 90.56, 90
Resolution (Å)	29.4 - 3.2 (3.420-3.2)	29.67 - 2.9 (3.004 - 2.9)	28.86 - 3.1 (3.311 - 3.1)	29.66 - 2.66 (2.76 - 2.66)	29.62 - 2.83 (2.931 - 2.83)	128 – 3.35 <sup>a</sup> 65.2 - 3.35 <sup>b</sup> (3.47-3.35)
Total no. of observations	73637 (13700)	110563 (18582)	144955 (26928)	218095 (14311)	180794 (11859)	64231 (9693)
No. of unique observations	19627 (3564)	24697 (3978)	21458 (3884)	31505 (2074)	26309 (1817)	17652 (2542)
Multiplicity	3.8 (3.8)	4.5 (4.7)	6.8 (6.9)	6.9 (7.0)	6.9 (6.5)	3.6 (3.8)
Data completeness (%)	98 (99)	100 (100)	100 (100)	99 (91)	99 (94)	99 (100)
$I/\sigma_I$	6.7 (1.7)	6.8 (1.9)	11.5 (4.8)	11.6 (1.9)	11.9 (2.1)	6.8 (2.4)
$R_{\text{merge}}$	0.14 (0.69)	0.15 (0.72)	0.11 (0.31)	0.11 (0.76)	0.12 (0.87)	0.16 (0.53)
<b>Refinement</b>						
Non-hydrogen atoms						
Protein	5916	6133	6070	6077	6100	5982
Water	0	0	0	13	0	0
$R_{\text{work}}/R_{\text{free}}$	0.232/0.278	0.217/0.272	0.219/0.265	0.230/0.270	0.219/0.263	0.232/0.272
r.m.s. deviations						
Bond lengths (Å)	0.008	0.011	0.004	0.004	0.013	0.005
Bond angles ( $^{\circ}$ )	1.14	0.9	0.71	0.71	1.31	0.74
Ramachandran plot (%)						
Favored	91	93	93	94	94	93
Allowed	8.9	6.3	6.2	5.5	6.1	7
Disallowed	0.13	0.26	0.38	0.26	0.26	0

Values in parentheses refer to the highest resolution shell for each dataset. <sup>a</sup> resolution range for data collection <sup>b</sup> resolution range for refinement